Scaling analysis of thin plate-like acoustic metamaterials

Jaeho Cho[a] and Felix Langfeldt[a*]

[a]Institute of Sound and Vibration Research, University of Southampton, University Road, Highfield, Southampton, SO17 1BJ, United Kingdom

---

[*]Corresponding author: Felix Langfeldt, Institute of Sound and Vibration Research, University of Southampton, University Road, Highfield, Southampton, SO17 1BJ, United Kingdom. E-mail address: F.Langfeldt@soton.ac.uk, Tel: +44-23-8059-4933

Abstract

We present a scaling analysis method for the sound transmission loss of thin acoustic metamaterial plates which can achieve high transmission loss at certain frequencies. The practical design and experimental validation of such metamaterial plates often faces challenges due to dimensional sensitivities and constraints dictated by experimental equipment and computational resources. To address this, a scaling analysis method is proposed which establishes simple relationships between the sound transmission loss of geometrically scaled acoustic metamaterial plates. Scaling formulas are derived mathematically based on the plate equation with variable bending stiffness and three scaling cases are considered: complete scaling, mass-neutral scaling, and thickness scaling. The scaling relationships are validated using finite element simulations of different plate-type acoustic metamaterial examples (i.e., thin plates with periodically attached rigid masses). The proposed scaling relationships will be valuable in simplifying the design of acoustic metamaterial plates, speeding up numerical optimizations, or enabling scaled-down acoustic experiments.

Key words: scaling analysis; structural waves; acoustic metamaterial; plate; unit cell; transmission loss.

1. Introduction

Acoustic metamaterials are artificially engineered materials that can control waves propagating through a medium [1-3]. Acoustic metamaterials can exhibit unusual properties, such as negative effective density or bulk modulus, which cannot be found in nature. Recently, various studies have been reported on acoustic metamaterial plates, which utilize acoustic metamaterials in soundproofing panel designs to achieve high sound transmission loss (STL) [4-24]. These plates include several types: where local resonators functioning as mass-spring systems are attached to a plate to reduce vibration [4-8], designs that combine acoustic resonators with a plate to reduce noise through acoustic resonances [9-11], sandwich panels made up of top and bottom plates with meticulously designed pathways between them [12-15], plate structures integrated with periodic stub or pillar attachments made of heavy metal or rubber materials to control flexural waves by forming band gaps in targeted frequency ranges [16-18], and plate-type acoustic metamaterials (PAMs) composed of rigid masses periodically distributed on a thin plate achieving noise reduction from their anti-resonances [19-24]. These acoustic metamaterial plates have gained significant attention due to their ability to reduce sound and vibration effectively without relying on thick and heavy materials (e.g. conventional panels), which are governed by the mass-law.

Despite these advantages, several challenges arise in the design and experimental validation phase: The noise attenuation characteristics of acoustic metamaterial plates are highly related to the geometry of the unit cell design, such as the mass shape, size, and thickness in PAMs. These relationships are particularly complicated when broadband sound transmission loss improvements are desired, e.g. by designing multi-modal local resonators [7,8] or using PAM designs with multiple masses in a single unit cell [20].

When geometrical dimensions required to position anti-resonances within the desired frequency range are unknown, iterative calculations are often necessary, leading to considerable time consumption. Furthermore, during experimental validation using sound transmission loss tests, the maximum test sample size can be limited by the experimental facilities.

A solution to these challenges can be found in the scaling and similitude analysis method. Scaling or similitude analysis investigates the effects of altering the size of a structure on its performance and establishes relationships between original and scaled geometries through governing equations or dimensionless parameters [25,26]. A well-known example for the benefits of scaling can be found in fluid dynamics, where Reynolds similarity is exploited in both experimental and computational applications. In structural dynamics, methodologies for correlating dynamic characteristics using scaling or similitude analysis have been proposed [27-31]. However, applying scaling analysis methods to the analysis and prediction of the sound insulation characteristics of acoustic metamaterial plates has not yet been reported.

In this letter, we introduce a scaling analysis method for the sound transmission loss of thin acoustic metamaterial plates, enabling the prediction of the sound insulation performance of scaled metamaterial plates based on results for the original geometry. We consider two types of scaling coefficients (in-plane and out-of-plane) and mathematically derive scaling relationships for the sound transmission loss using a PAM as an example. Based on this, three scaling cases are considered: Complete scaling, which scales the unit cell geometry equally in all three spatial directions; mass-neutral scaling, which preserves the total mass of the metamaterial; and thickness scaling, which only changes the overall thickness of the metamaterial. The effectiveness of the proposed scaling analysis method is validated using finite element simulations.

2. Modeling and method

In this section, we introduce the analytical scaling law for the sound transmission loss of thin plate-like acoustic metamaterials. The derivation is based on the assumptions of normal incidence of acoustic waves, infinite periodicity of the metamaterials in the in-plane directions, sub-wavelength size of the metamaterial unit cells, and the applicability of the Kirchhoff-Love plate theory, which requires the plate to be thin relative to its lateral dimensions.

2.1. Analysis model and sound transmission characteristics of PAMs

Fig. 1 shows an example configuration of a PAM and the unit cell comprising it. In this example, each unit cell, shown on the right, consists of a plate with a circular mass attached on its top, and the PAM is configured with these unit cells periodically arranged along the x and y directions as defined in the three-dimensional Cartesian coordinate system (x, y, z) shown on the left. It should be noted that the configuration shown in Fig. 1 has been chosen for simplicity – the analysis proposed in this paper also applies to more complicated acoustic metamaterial plate designs, e.g. PAMs with multiple masses in a unit cell or more complicated mass geometries. Without loss of generality, the unit cell lengths in both the x and y directions are assumed to be equal (a) and the thickness of the plate is denoted as h_p. The diameter and height of the circular mass positioned in the center of the unit cell are denoted as d_M and h_M, respectively. The frequency-dependent characteristics of PAMs can be identified from the effective surface mass density (m''_{eff}), which is defined as follows [32]:

$$m''_{\mathrm{eff}}(f) = \frac{p}{-(2\pi f)^2 \langle w(f) \rangle}, \tag{1}$$

where f is the frequency, $\langle w(f) \rangle$ indicates the surface-averaged complex normal displacement amplitude of the PAM in response to a uniform pressure p applied to the PAM. In general, the normal displacement of a thin plate is governed by the Kirchhoff-Love plate equation. The displacement field of the PAM can be calculated using the plate equation with variable bending stiffness [33]:

$$\left(\frac{\partial^2}{\partial x^2}\left(D\left(\frac{\partial^2}{\partial x^2} + \nu \frac{\partial^2}{\partial y^2}\right)\right) + 2\frac{\partial^2}{\partial x \partial y}\left(D(1-\nu)\frac{\partial^2}{\partial x \partial y}\right) + \frac{\partial^2}{\partial y^2}\left(D\left(\frac{\partial^2}{\partial y^2} + \nu \frac{\partial^2}{\partial x^2}\right)\right) - \rho h (2\pi f)^2\right) w = p, \tag{2}$$

where D indicates the local bending stiffness, defined as $D = Eh^3/(12(1-\nu^2))$, E, ν, ρ, and h are the local Young's modulus, Poisson's ratio, density, and thickness (equal to h_p or $h_p + h_M$), depending on the location within the unit cell, respectively. Once the effective surface mass density is known, the noise attenuation characteristics of the PAM can be evaluated through the frequency-dependent STL, which is derived from the sound transmission factor (t) via [34]:

$$t(f) = \left(1 + \frac{\mathrm{i}(2\pi f)}{2\rho_0 c_0} m''_{\mathrm{eff}}(f)\right)^{-1}, \ \mathrm{i} = \sqrt{-1}, \tag{3a}$$

$$\mathrm{TL}(f) = -20 \log_{10} |t(f)|, \tag{3b}$$

where ρ_0 and c_0 are the density and speed of sound of the acoustic medium surrounding the PAM, respectively.

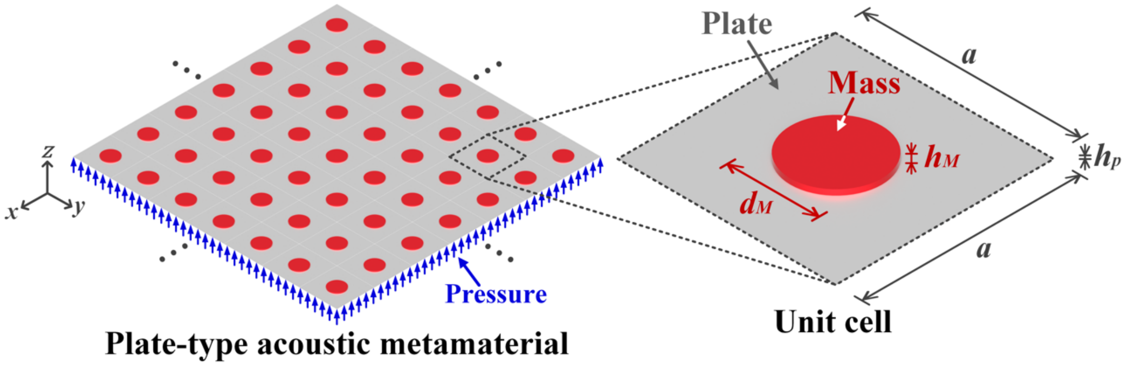

Fig. 1 Configuration of a PAM with a unit cell composed of circular mass

2.2. *Derivation of the scaling law*

As the dimensions of the PAM unit cell change, the displacement field w will be altered and the STL varies correspondingly. To establish a relationship between the STL of scaled and original PAMs, a scaling law based on Eq. (2) is derived. Starting from the original coordinate system, defined as x, y, and z, when the in-plane dimensions (x- and y-directions) are scaled by γ_a and the thickness of the plate and height of the mass are equally scaled by γ_h, the new coordinate system of the scaled geometry can be denoted as x_s, y_s, and z_s, with the relationships between the scaled and original coordinates given by

$$x_s = \gamma_a x,\ y_s = \gamma_a y, \tag{4a}$$

$$h_s = \gamma_h h, \tag{4b}$$

If the material composition of the scaled metamaterial remains identical to the original design, the plate equation in Eq. (2) can be rewritten in terms of the scaled coordinate system as follows:

$$\left(\frac{\partial^2}{\partial x_s^2}\left(D_s\left(\frac{\partial^2}{\partial x_s^2}+\nu\frac{\partial^2}{\partial y_s^2}\right)\right)+2\frac{\partial^2}{\partial x_s\partial y_s}\left(D_s(1-\nu)\frac{\partial^2}{\partial x_s\partial y_s}\right)+\frac{\partial^2}{\partial y_s^2}\left(D_s\left(\frac{\partial^2}{\partial y_s^2}+\nu\frac{\partial^2}{\partial x_s^2}\right)\right)-\rho h_s(2\pi f_s)^2\right)w_s=p, \quad (5)$$

where w_s, f_s, and h_s represent the normal displacement, frequency, and local thickness of the scaled PAM, respectively. Along with the coordinate scaling, the partial differential notation was modified correspondingly. Although the material composition remains constant, the local bending stiffness of the PAM is affected by the thickness scaling ratio (γ_h), resulting in $D_s=\frac{Eh_s^3}{12(1-\nu^2)}$. Based on the relationships in Eq. (4a), the partial differential operators of the scaled geometry can be expressed as

$$\partial x_s=\gamma_a\partial x,\ \partial y_s=\gamma_a\partial y, \quad (6)$$

Additionally, from Eq. (4b) it follows that the bending stiffnesses of the original and scaled PAM follow the relationship

$$D_s=\frac{E}{12(1-\nu^2)}h_s^3=\gamma_h^3\frac{E}{12(1-\nu^2)}h^3=\gamma_h^3 D. \quad (7)$$

By inserting Eqs. (6) and (7) in Eq. (5), the plate equation of the scaled metamaterial can be expressed as follows:

$$\left(\frac{\partial^2}{\partial x^2}\left(D\left(\frac{\partial^2}{\partial x^2}+\nu\frac{\partial^2}{\partial y^2}\right)\right)+2\frac{\partial^2}{\partial x\partial y}\left(D(1-\nu)\frac{\partial^2}{\partial x\partial y}\right)+\frac{\partial^2}{\partial y}\left(D\left(\frac{\partial^2}{\partial y^2}+\nu\frac{\partial^2}{\partial x^2}\right)\right)-\rho h\left(\frac{\gamma_a^2}{\gamma_h}(2\pi f_s)\right)^2\right)\frac{\gamma_h^3}{\gamma_a^4}w_s=p. \quad (8)$$

When comparing Eqs. (2) and (8), differences exist only in the terms related to the frequency (f and f_s) and the normal displacement (w and w_s); all other terms remain identical. This indicates that the displacement and corresponding frequency calculated or measured on the scaled geometry can be scaled to match that of the original geometry by using the following scaling relationships:

$$f = \frac{\gamma_a^2}{\gamma_h} f_s, \tag{9a}$$

$$w = \frac{\gamma_h^3}{\gamma_a^4} w_s, \tag{9b}$$

From these displacement and frequency scaling relationships, the definition of the effective surface mass density is used to derive a scaling law for the STL of the scaled PAM, relating its STL to that of the original PAM. Following the definition in Eq. (1), the effective surface mass density of the scaled PAM $\left(m''_{\mathrm{eff}_s}\right)$ is expressed as

$$m''_{\mathrm{eff}_s}(f_s) = \frac{p}{-(2\pi f_s)^2 \langle w_s(f_s) \rangle}, \tag{10}$$

Substituting the relevant terms from Eq. (9), this can be rewritten as

$$m''_{\mathrm{eff}_s}(f) = \gamma_h \frac{p}{-(2\pi f)^2 \langle w(f) \rangle} = \gamma_h m''_{\mathrm{eff}}(f), \tag{11}$$

which provides a direct scaling relationship between the scaled and original PAM at the same frequency f. It should be noted that even though the metamaterial was scaled based on two coefficients, the terms involving γ_a in the scaling relationships for f_s and w_s involving γ_a canceled each other out, resulting in the effective surface mass density of the scaled geometry depending solely on the out-of-plane scaling factor γ_h. This is consistent with the case of a homogeneous plate where the surface mass density is independent of frequency and only changes when the thickness of the plate is scaled.

Using Eqs. (9a) and (11), the sound transmission factor of the scaled metamaterial (t_s) is given by

$$t_s(f) = \left(1 + \frac{\mathrm{i}(2\pi f_s)}{2\rho_0 c_0} m''_{\mathrm{eff}_s}(f)\right)^{-1} = \left(1 + \left(\frac{\gamma_h}{\gamma_a}\right)^2 \frac{\mathrm{i}(2\pi f)}{2\rho_0 c_0} m''_{\mathrm{eff}}(f)\right)^{-1}. \tag{12}$$

Using Eq. (3a), Eq. (12) can be rearranged to establish the following relationship between the sound transmission factors of the scaled and original metamaterials:

$$t(f) = \left(1 + \left(\frac{\gamma_a}{\gamma_h}\right)^2 \left(\left(t_s(f)\right)^{-1} - 1\right)\right)^{-1}. \tag{13}$$

By substituting this result into Eq. (3b), the rescaled transmission loss ($\widehat{\mathrm{TL}}(f)$) can be obtained from the sound transmission factor of the scaled geometry t_s:

$$\widehat{\mathrm{TL}}(f) = -20\log_{10}\left|\left(1 + \left(\frac{\gamma_a}{\gamma_h}\right)^2 \left(\left(t_s(f)\right)^{-1} - 1\right)\right)^{-1}\right|. \tag{14}$$

The notation $\widehat{\mathrm{TL}}(f)$ has been introduced to make a clear distinction between the STL of the original metamaterial ($\mathrm{TL}(f)$) and the rescaled STL calculated via Eq. (14) and using transmission factor values of the scaled metamaterial (obtained using, for example, numerical simulations or experiments). It should be noted that Eq. (14) is also valid for homogeneous plates, although not immediately obvious because γ_a appears in Eq. (14), which should not affect the STL in case of a homogeneous plate. However, when assuming a frequency-independent surface mass density, inserting Eq. (12) in Eq. (14) cancels the dependency on γ_a, as would be expected for homogeneous plates.

3. Numerical validation and discussion

To validate the proposed method, three scaling cases are considered based on the two scaling coefficients γ_a and γ_h: (1) scaling in all directions (x, y, z) (complete scaling), (2) scaling in-plane dimensions only (x, y) while the height remains identical ($\gamma_h = 1$) (mass-neutral scaling), and (3) only scaling out-of-plane dimensions (z) while the in-plane dimensions remain identical ($\gamma_a = 1$) (thickness scaling). As a representative example, the PAM shown in Fig. 1 with material parameters and dimensions based on [35] was used as the original design. The plate material was polycarbonate ($E = 2.3$ GPa, $\nu = 0.40$, $\rho = 1310\ \mathrm{kg/m^3}$) with a structural loss factor of 5%. The mass was made of steel ($E = 205$ GPa, $\nu = 0.28$, $\rho = 7850\ \mathrm{kg/m^3}$) with a structural loss factor of 1%. The acoustic medium was air ($\rho_0 = 1.23\ \mathrm{kg/m^3}$, $c_0 = 343\ \mathrm{m/s}$). The numerical analysis was conducted based on the finite element method (FEM) using COMSOL Multiphysics (ver. 6.2), and the simplified metamaterial plate modeling method described in Ref. [36] was followed to calculate the STL. Further details of the numerical simulation setup are provided in Appendix A. For a finite array, the dynamic behavior converges to that of an infinite array once a sufficient number of unit cells are used, as shown in Ref. [35]. Therefore, the scaling relationships derived in this letter are expected to remain valid even for finite acoustic metamaterial plates of practical size.

Fig. 2(a) shows the STL curves of the original and scaled PAMs calculated via finite element simulations using complete scaling (i.e., $\gamma_a = \gamma_h$). In this case, the geometry is scaled uniformly in all directions and the dimensions of the scaled and original geometries are detailed in Table 1, including the corresponding static surface mass density (μ) of each configuration. The STL of the original PAM is represented by the black dash-dotted line. Between 100 to 1000 Hz, two anti-resonances are observed in the form of STL peaks. The first anti-resonance occurs at 257 Hz with a STL of 27.4 dB and the second anti-resonance at 670 Hz with a STL of 22.9 dB. From observing the STL curves of the scaled PAMs, it can be seen that if the scaling factors increase (i.e., the unit cell becomes bigger), the anti-resonance frequencies shift to lower frequencies, while they shift to higher frequencies if the scaling factors decrease. However, the STL values at both anti-resonance frequencies remain at the same level, regardless of the scaling. For example, when $\gamma_a = \gamma_h = 3$, the first and second anti-resonances shift to 85.7 Hz and 223.3 Hz, with corresponding STL values of 27.4 dB and 22.9 dB, respectively. Conversely, when $\gamma_a = \gamma_h = 1/3$, the anti-resonances shift to 771 Hz and 2010 Hz, with STL values of 27.4

dB and 22.9 dB. This behavior aligns with Eq. (14), where γ_a and γ_h cancel each other out when they are equal, resulting in consistent STL values for complete scaling. Therefore, complete scaling can be useful, for example, to achieve a fixed STL level at different anti-resonance frequencies by scaling the unit cell geometry according to the frequency scaling law given in Eq. (9a), which reduces to $f = \gamma_a f_s$ in the case of complete scaling. Fig. 2(b) shows the STL curves that have been analytically rescaled by applying the scaling law in Eq. (14) to the FEM results of the scaled PAMs. Despite the high range of scaling factors, ranging from 1/3 to 3, and the different materials used in the PAM designs, the rescaled TL curves exhibit remarkable consistency with almost no visible differences. Fig. 3 shows the normal displacement fields of each scaled PAM at their respective anti-resonance frequencies. For both the first and second anti-resonance, it can be observed that the locations of high and low displacement regions remain identical across different scaling factors.

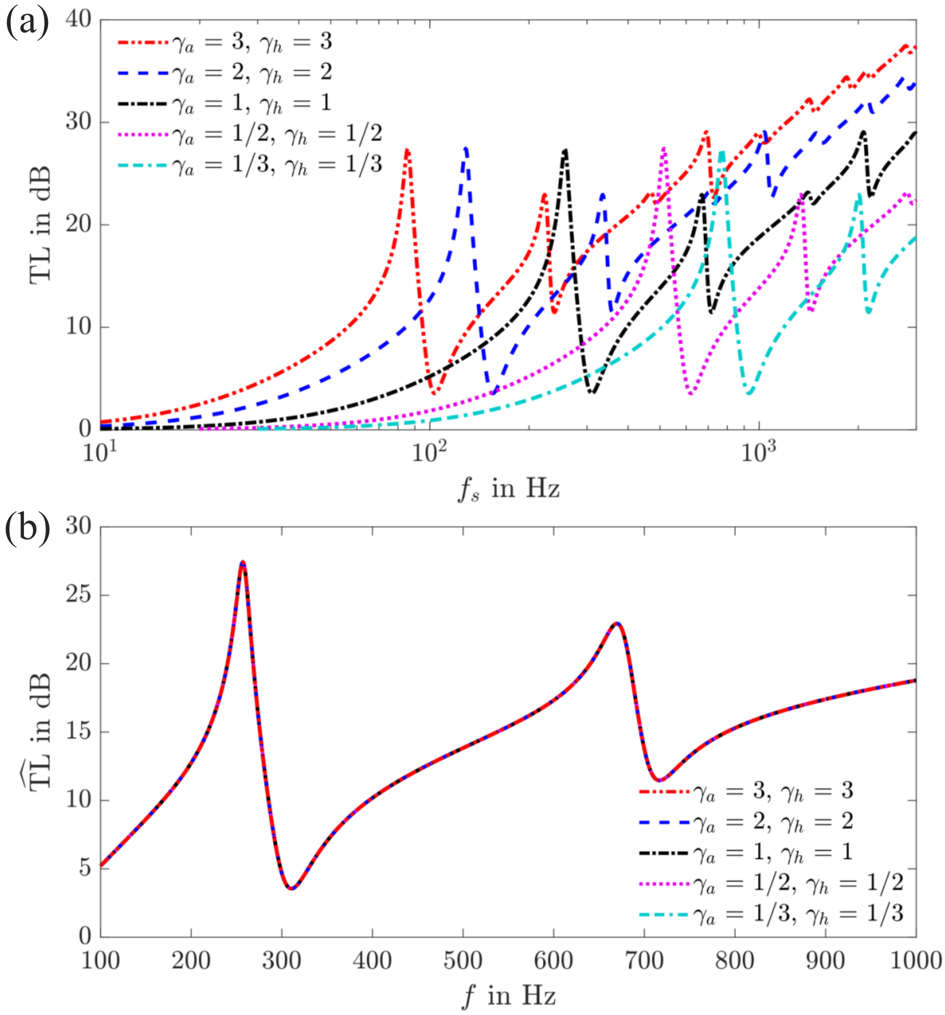

Fig. 2 STL curves of the original and scaled PAMs with complete scaling ($\gamma_a = \gamma_h$): (a) STL curves calculated via FEM, plotted against the frequency f_s of the scaled PAM and (b) STL curves analytically rescaled by applying the scaling law in Eq. (14) to the FEM results, plotted against the rescaled frequency f.

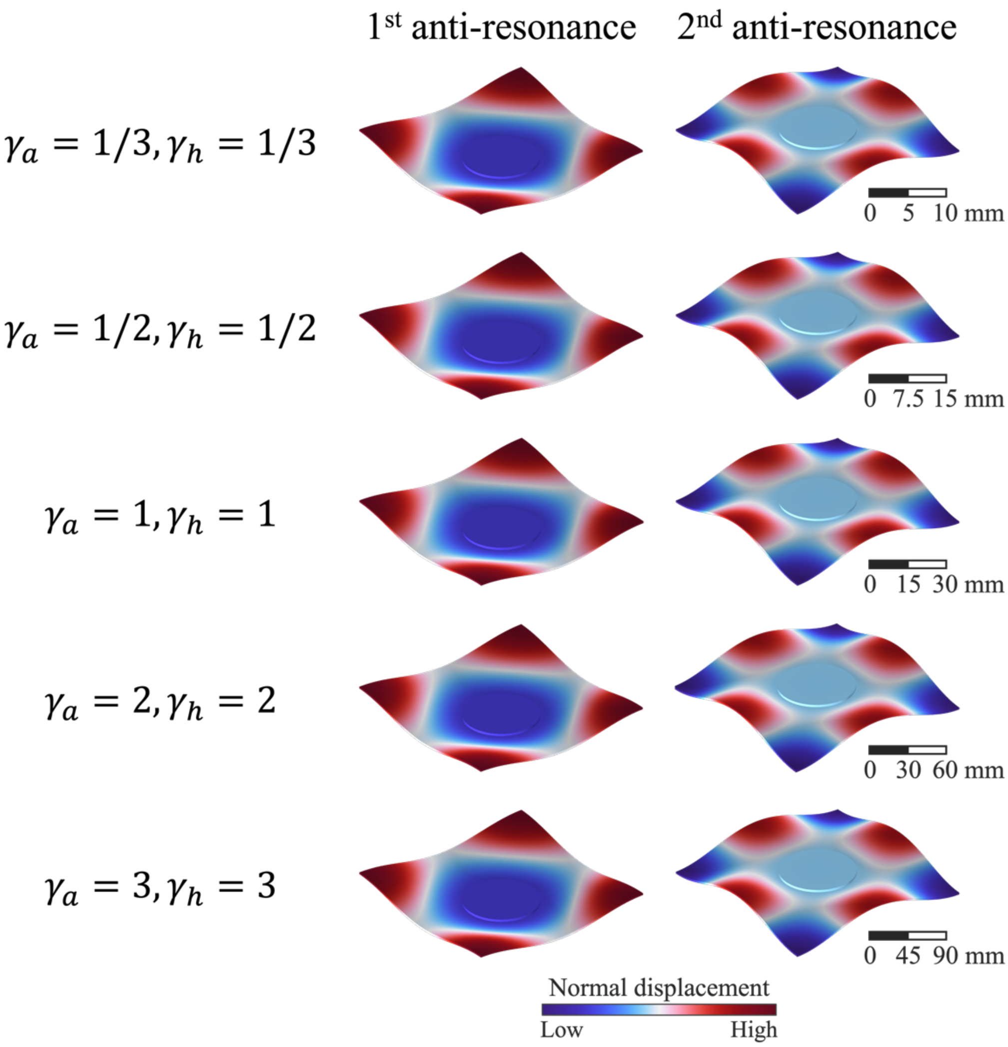

Fig. 3 Normal displacement fields of the scaled PAMs in complete scaling.

Table 1 Dimensions of the original and scaled PAMs using complete scaling (original PAM: $\gamma_a = 1,\ \gamma_h = 1$).

γ_a	γ_h	a (mm)	d_M (mm)	h_p (μm)	h_M (mm)	μ (g/m^2)
1/3	1/3	25.83	10	250	0.333	635
1/2	1/2	38.75	15	375	0.5	953
1	1	77.5	30	750	1	1906
2	2	155	60	1500	2	3813
3	3	232.5	90	2250	3	5719

In some applications it is desirable to alter the anti-resonance frequencies of a metamaterial plate without changing the overall (static) mass of the metamaterial. This leads to the case of mass-neutral scaling, for which the static surface mass density remains constant. This is achieved if γ_h remains at 1 while only γ_a is varied, i.e. the thickness of the metamaterial plate remains constant and only the in-plane dimensions are adjusted. Fig. 4(a) shows the STL of the scaled PAMs with mass-neutral scaling, calculated via finite element simulations. The corresponding dimensions of the scaled PAMs are summarized in Table 2, also demonstrating how the static surface mass density μ remains constant in this case. As shown in Fig. 4(a) and as follows from Eq. (9a), if γ_a increases, the anti-resonance frequency decreases (according to $f = \gamma_a^2 f_s$), along with a corresponding decrease in the STL values (because now the γ_a and γ_h do not cancel in Eq. (14)). Conversely, if γ_a decreases, the anti-resonance frequency increases, and the STL values increase. For instance, when $\gamma_a = 3$, the first and second anti-resonances shift to 28.8 Hz and 75.2 Hz, with STL values of 10.9 dB and 7.4 dB, respectively. In contrast, when $\gamma_a = 1/3$, the first and second anti-resonances shift to 2251 Hz and 5851 Hz, with STL values of 46.1 dB and 41.1 dB, respectively. Fig. 4(b) shows the STL curves analytically rescaled by applying Eq. (14) to the FEM results from mass-neutral scaling. Overall, the rescaled STL values exhibit good agreement, in particular for scaled PAMs with high γ_a values. In contrast, for low values of γ_a, gradually increasing differences are observed as γ_a decreases. Fig. 5 shows the normal displacement fields of each scaled PAM under mass-neutral scaling at their respective anti-resonance frequencies. As γ_a decreases, it can be seen that the relative heights of the mass and plate increase compared to the unit cell length. For both the first and second anti-resonance, the locations of high and low displacement regions remain almost identical across different scaling factors, despite the variations in geometry.

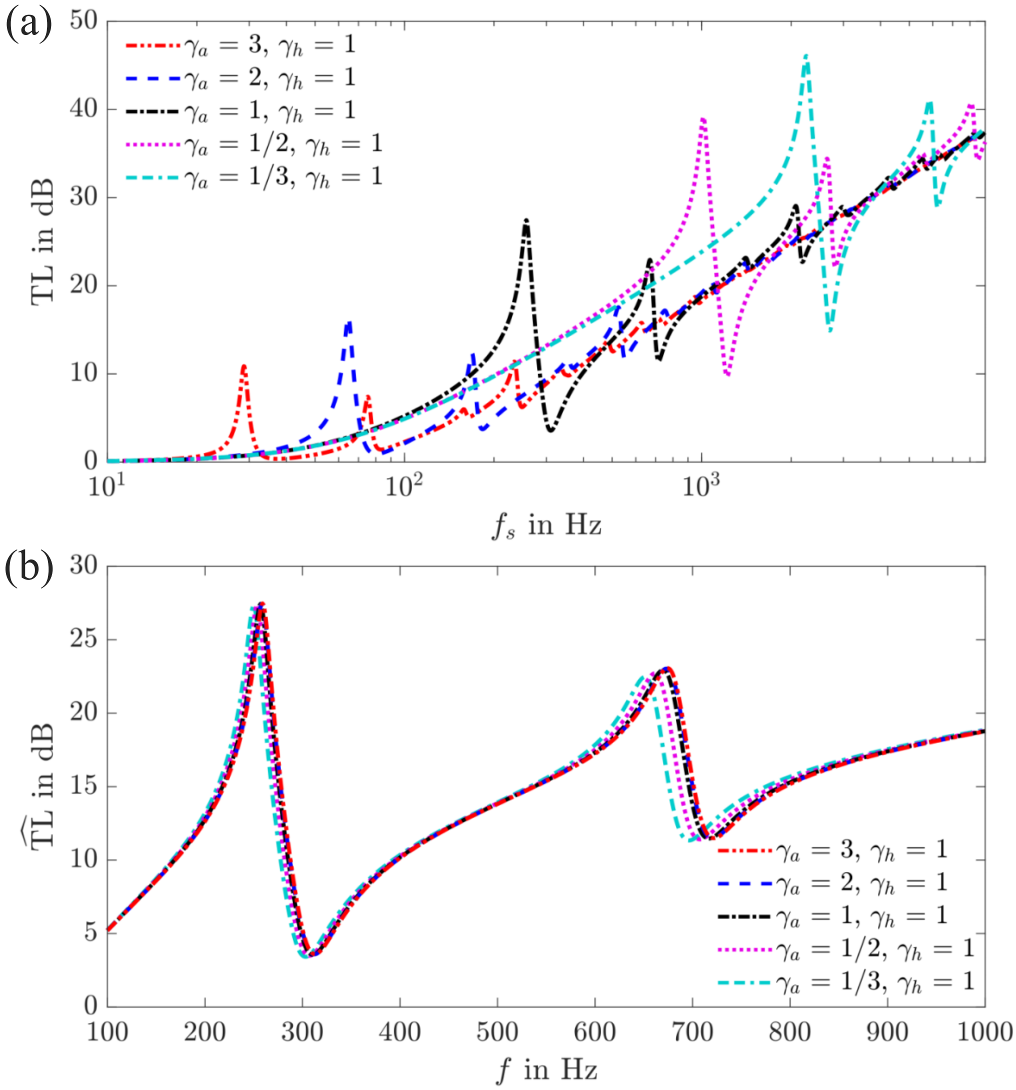

Fig. 4 STL curves of the original and scaled PAMs with mass-neutral scaling $(\gamma_h = 1)$: (a) STL curves calculated via FEM, plotted against the frequency f_s of the scaled system and (b) STL curves analytically rescaled by applying the scaling law in Eq. (14) to the FEM results, plotted against the rescaled frequency f.

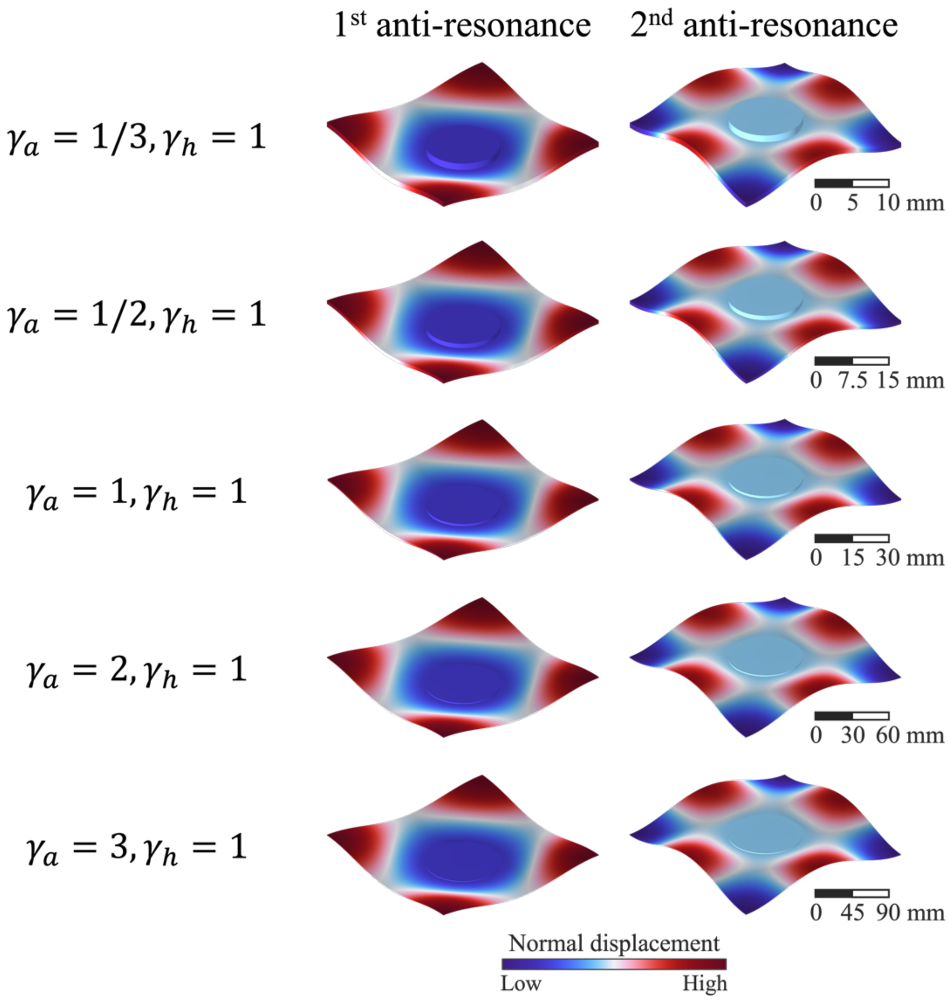

Fig. 5 Normal displacement fields of the scaled PAMs in mass-neutral scaling.

Table 2 Dimensions of the original and scaled PAMs using mass-neutral scaling (original PAM: $\gamma_a = 1,\ \gamma_h = 1$).

γ_a	γ_h	a (mm)	d_M (mm)	h_p (μm)	h_M (mm)	μ (g/m^2)
1/3	1	25.83	10	750	1	1906
1/2	1	38.75	15	750	1	1906
1	1	77.5	30	750	1	1906
2	1	155	60	750	1	1906
3	1	232.5	90	750	1	1906

Another scaling case that can be considered using the proposed method is thickness scaling, for which the in-plane dimensions remain constant while only γ_h varies, thereby only adjusting the thickness of the metamaterial. Fig. 6(a) shows the STL curves of the PAMs with thickness scaling, calculated via finite element simulations. The dimensions and static surface mass densities of the thickness-scaled PAMs are summarized in Table 3. The results show that by decreasing γ_h (resulting in a thinner, more lightweight PAM), the anti-resonance frequencies decrease according to $f = \gamma_h^{-1} f_s$. Conversely, when γ_h increases (resulting in a thicker, heavier PAM), the anti-resonance frequencies shift to higher frequencies. Furthermore, the STL values decrease as γ_h decreases and vice versa. For instance, when $\gamma_h = 1/3$, the first and second anti-resonances shift to 86.3 Hz and 225.7 Hz, with STL values of 10.9 dB and 7.4 dB, respectively. In contrast, when $\gamma_h = 3$, the first and second anti-resonances shift to 748 Hz and 1951 Hz, with STL values of 46.1 dB and 41.1 dB, respectively. Fig. 6(b) shows the STL curves analytically rescaled by applying Eq. (14) to the FEM results of the thickness scaled PAMs. When $\gamma_h < 1$, the results for the rescaled STL align closely with the STL curve of the original PAM. However, when γ_h is set higher than 1, the rescaled STL curve starts to deviate from the original PAM STL. Fig. 7 shows the normal displacement fields of each scaled PAM under thickness scaling at their respective anti-resonance frequencies. As γ_h increases, the heights of the mass and plate increase compared to the unit cell length. For both the first and second anti-resonance, the locations of high and low displacement regions remain almost identical across different scaling factors, despite the variations in geometry.

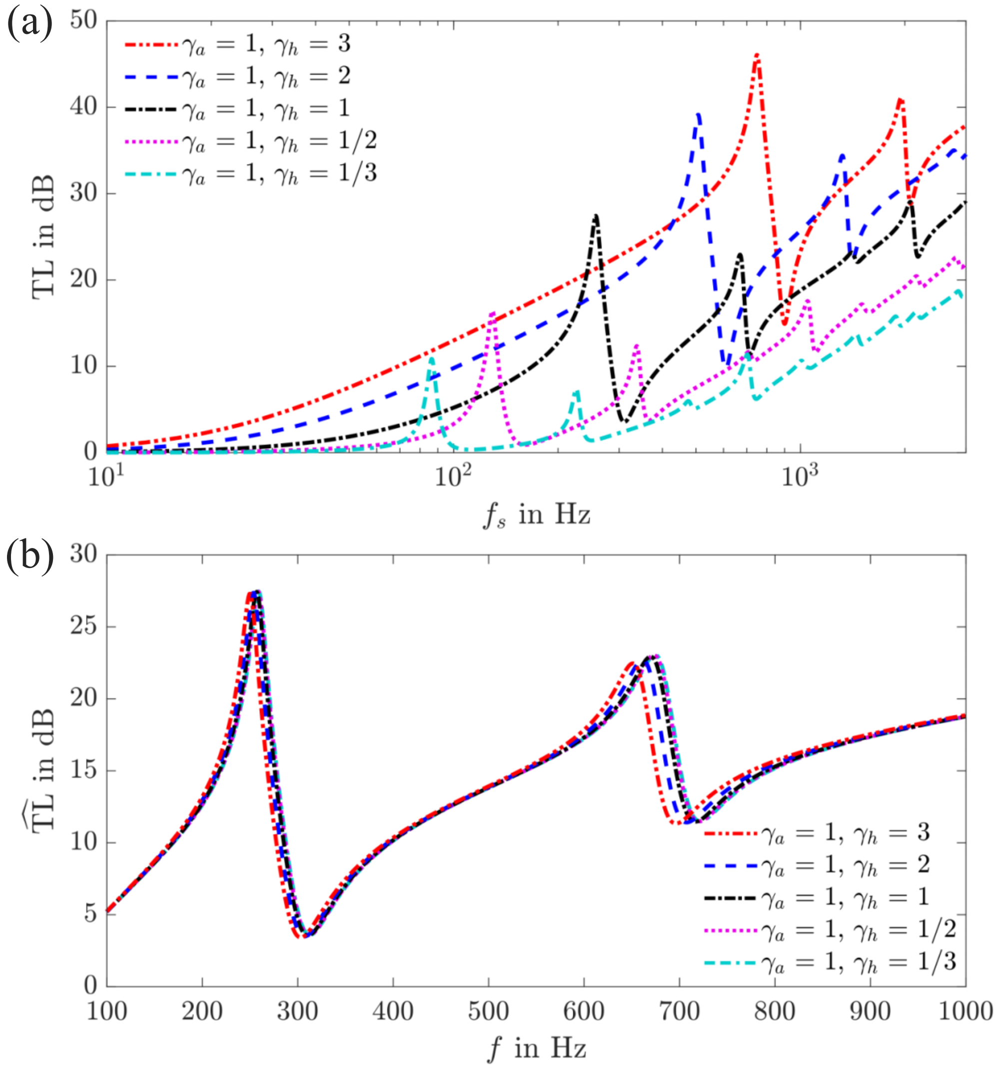

Fig. 6 STL curves of the original and scaled PAMs with thickness scaling $(\gamma_a = 1)$: (a) STL curves calculated via FEM, plotted against the frequency f_s of the scaled PAMs and (b) STL curves analytically rescaled by applying the scaling law in Eq. (14) to the FEM results, plotted against the rescaled frequency f.

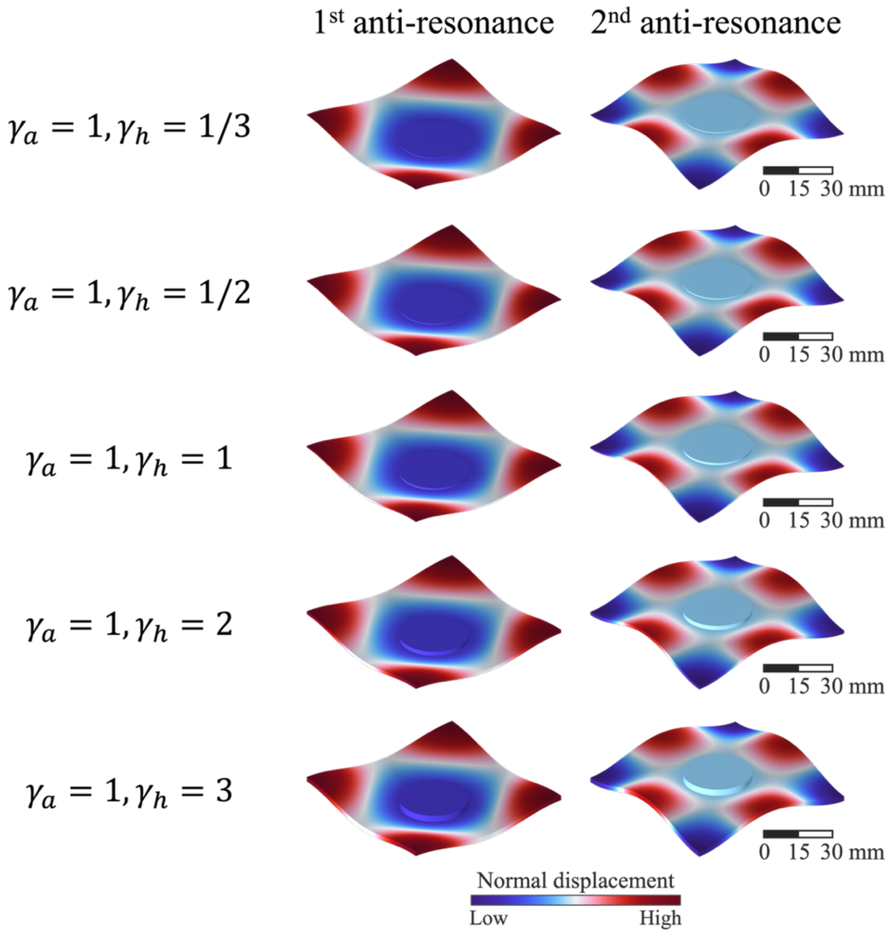

Fig. 7 Normal displacement fields of the scaled PAMs in thickness scaling.

Table 3 Dimensions of the original and scaled PAMs using thickness scaling (original PAM: $\gamma_a = 1$, $\gamma_h = 1$).

γ_a	γ_h	a (mm)	d_M (mm)	h_p (μm)	h_M (mm)	μ (g/m^2)
1	1/3	77.5	30	250	0.333	635
1	1/2	77.5	30	375	0.5	953
1	1	77.5	30	750	1	1906
1	2	77.5	30	1500	2	3813
1	3	77.5	30	2250	3	5719

To further analyze the validity and limits of the proposed scaling method, additional calculations were conducted for the two scaling cases for which discrepancies were observed. Fig. 8(a) shows the absolute difference between the STL of the original PAM (TL) and of the scaled PAMs ($\widehat{\mathrm{TL}}$) with mass-neutral scaling. Here, γ_a was varied from 1 to 0.3, with an interval of 0.01. When γ_a decreases from 1 to 0.77, the errors in the rescaled STL are almost negligible, remaining within 1 dB. However, for γ_a as low as 0.55, the observed differences begin to exceed 3 dB at 686 Hz, and starting from $\gamma_a = 0.39$, discrepancies of more than 6 dB are observed at 683 Hz. Fig. 8(b) shows the absolute difference between the original STL and $\widehat{\mathrm{TL}}$ with thickness scaling. Here, γ_h was varied from 1 to 3, with an interval of 0.02. For γ_h between 1 and 1.3, the errors in the rescaled STL are within 1 dB. However, for γ_h exceeding 1.82, discrepancies larger than 3 dB can be observed at 685 Hz, and discrepancies larger than 6 dB are observed at 682 Hz if $\gamma_h > 2.56$.

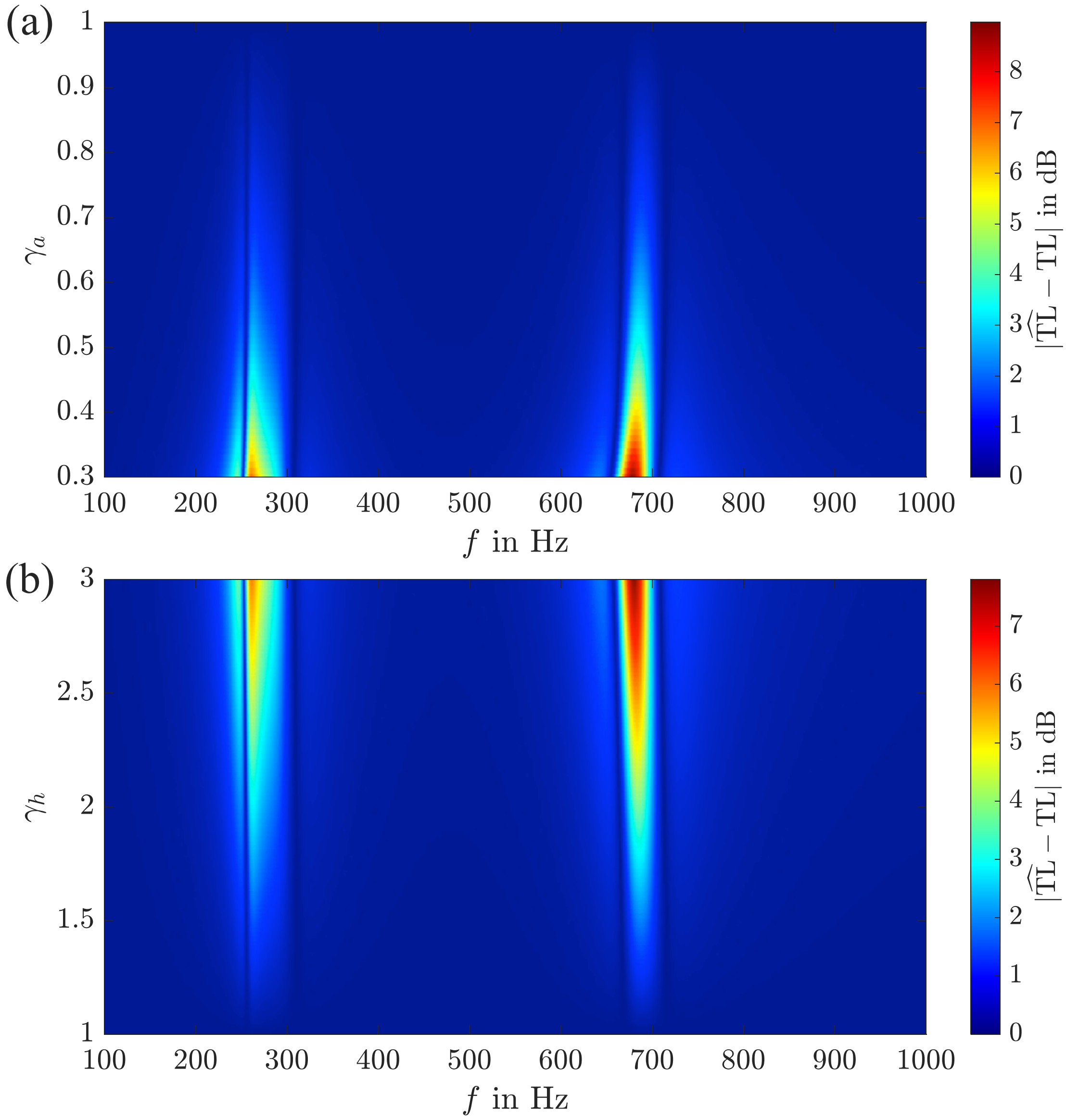

Fig. 8 Difference between the original PAM STL and the rescaled STL for different scaling approaches: (a) mass-neutral scaling and (b) thickness scaling.

The increasing discrepancies for small γ_a (mass-neutral scaling) or large γ_h (thickness scaling) can be explained as follows: In these cases, the plate and mass become considerably thick compared to the unit cell length a of the PAMs. The scaling analysis method proposed in this letter was derived mathematically based on the Kirchhoff-Love plate equation with variable bending stiffness, which assumes that the thickness of the plate is much smaller than the lateral dimensions (a). If this is violated, dynamic characteristics, such as in-plane motion or torsion, which were not considered during the derivation of the plate equation, become non-negligible, and the error in the rescaled STL increases. One possible explanation can be found in the limitation of the Kirchhoff-Love plate theory, which does not account for transverse shear deformation or rotary inertia. As a result, the structural stiffness tends to be overestimated, since the theory assumes that the system does not respond to such effects. In contrast, real systems may exhibit these dynamic behaviors, and in such cases, the actual stiffness is lower than that estimated by the Kirchhoff-Love plate theory due to the presence of shear and rotational effects. In general, for a given mass, lower structural stiffness leads to lower characteristic frequencies. In cases where consistent discrepancies are observed, the rescaled STL exhibit a gradual downward shift in the anti-resonance frequency relative to the original STL. This trend aligns with the theoretical assumptions discussed above.

Nevertheless, even in the cases where discrepancies occurred, the rescaled STL curves exhibit relatively minor errors, despite considerable changes in dimensions. Additionally, the present scaling analysis incorporates material losses through the loss factors in both the plate (5%) and the mass (1%). Within the investigated range ($\leq 5\%$), the derived scaling law remains valid, indicating that moderate damping does not impair their applicability. For viscoelastic metamaterials that require higher loss factor, however, additional analysis may be required to extend the applicability of the proposed approach.

4. Conclusions

In this letter, a scaling analysis method for the sound transmission through acoustic metamaterial plates was proposed. Two types of scaling factors, in-plane and out-of-plane, were introduced and the scaling relationships between the frequencies and STL of the original and scaled metamaterial were established using the plate equation with variable bending stiffness. Based on the two scaling factors, three scaling cases were explored using numerical simulations of PAMs as an example for metamaterial plate: complete scaling, mass-neutral scaling, and thickness scaling. It could be shown that for complete scaling, a perfect agreement between the STL of the original and scaled metamaterial can be achieved using the proposed STL rescaling in Eq. (14). Minor discrepancies were observed in the mass-neutral and thickness scaling cases, which can be explained by the utilized thin plate-assumption being violated if the thickness becomes large compared to the unit cell size of the metamaterial. Nevertheless, even with substantial changes in the frequency range due to large variations in the scaling coefficients, the rescaled STL curves demonstrated a high degree of agreement with the original PAM.

The proposed scaling methodology can be applied to greatly simplify numerical or experimental studies of the sound transmission properties of acoustic metamaterial plates, like how Reynolds-similarity is exploited in fluid mechanics. While this letter focused on rescaling the STL of scaled metamaterial plates, the proposed method can also be reversed, which will allow to intentionally shift anti-resonances of a metamaterial plate to desired frequency ranges using the scaling formulas proposed in this letter. This will reduce the computational effort in designing complex metamaterial plate structures (e.g. using optimization procedures) and significantly simplify the tailoring of acoustic metamaterial plate designs towards different noise control applications with different problematic frequency ranges.

CRediT authorship contribution statement

Jaeho Cho: Methodology, Software, Validation, Formal analysis, Investigation, Data Curation, Writing - Original Draft, Writing - Review & Editing, Visualization.

Felix Langfeldt: Conceptualization, Resources, Writing - Review & Editing, Supervision, Project administration.

Declaration of competing interest

The authors declare that they have no known competing financial interests or personal relationships that could have appeared to influence the work reported in this paper.

Acknowledgments

The authors acknowledge the use of the IRIDIS High Performance Computing Facility, and associated support services at the University of Southampton, in the completion of this work. This research did not receive any specific grant from funding agencies in the public, commercial, or not-for-profit sectors.

Data availability

Data will be made available on request.

Appendix A: Details of finite element simulation

Fig. A.1(a) shows the meshed model used for the finite element simulation of the original PAM. The plate was modeled as a thin, uniform-thickness shell using two-dimensional shell elements, while the mass was modeled as a cylindrical geometry using three-dimensional solid elements. Quadratic shape functions were applied to both shell and solid elements. To simulate an infinitely periodic structure, periodic boundary conditions were applied to all four edges of the unit cell. Owing to the use of periodic boundary conditions, the global response of an infinite PAM can be obtained through the numerical analysis of a single unit cell. As illustrated in Fig. A1(b), at the overlapping boundaries of shell and solid, the shell and solid elements were rigidly connected via a solid-thin structure connection. A normally incident acoustic wave was simulated by applying a uniform pressure to the bottom of the PAM.

(a)

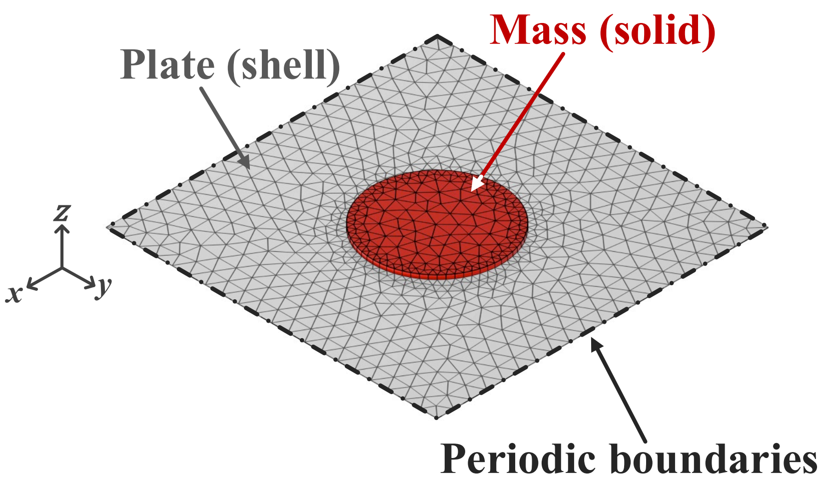

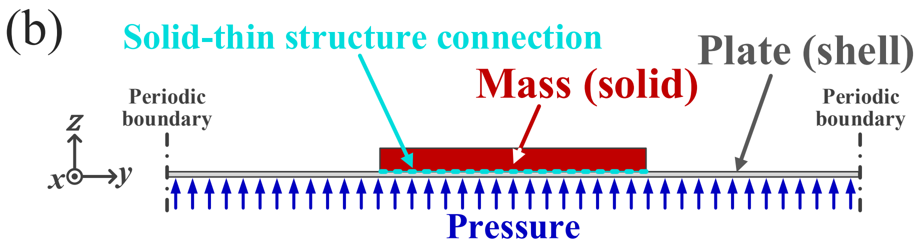

Fig. A.1. Schematic diagram of the numerical setup: (a) isometric view of the meshed model, (b) side view of the unit cell.

References

[1] J. Li, C.T. Chan, Double-negative acoustic metamaterial, Phys. Rev. E 70 (2004) 055602. https://doi.org/10.1103/PhysRevE.70.055602.

[2] S.H. Lee, C.M. Park, Y.M. Seo, Z.G. Wang, C.K. Kim, Acoustic metamaterial with negative density, Phys. Lett. A 373 (2009) 4464–4469. https://doi.org/10.1016/j.physleta.2009.10.013.

[3] G. Ma, P. Sheng, Acoustic metamaterials: From local resonances to broad horizons, Sci. Adv. 2 (2016). https://doi.org/10.1126/sciadv.1501595.

[4] Y. Xiao, J. Wen, X. Wen, Sound transmission loss of metamaterial-based thin plates with multiple subwavelength arrays of attached resonators, J. Sound Vib. 331 (2012) 5408–5423. https://doi.org/10.1016/j.jsv.2012.07.016.

[5] L. Van Belle, C. Claeys, E. Deckers, W. Desmet, The impact of damping on the sound transmission loss of locally resonant metamaterial plates, J. Sound Vib. 461 (2019) 114909. https://doi.org/10.1016/j.jsv.2019.114909.

[6] T. Wang, Tunable band gaps in an inertant metamaterial plate with two-degree-of-freedom local resonance, Phys. Lett. A 384 (2020) 126420. https://doi.org/10.1016/j.physleta.2020.126420.

[7] D. Giannini, E.P.B. Reynders, Effective medium modelling of real-world multi-modal metamaterial panels achieving broadband vibroacoustic attenuation, Extreme Mech. Lett. 69 (2024) 102161. https://doi.org/10.1016/j.eml.2024.102161.

[8] D. Giannini, M. Schevenels, E.P.B. Reynders, Topology optimization design of multi-modal resonators for metamaterial panels with maximized broadband vibroacoustic attenuation, J. Sound Vib. 595 (2025) 118691. https://doi.org/10.1016/j.jsv.2024.118691.

[9] T. Yamamoto, Acoustic metamaterial plate embedded with Helmholtz resonators for extraordinary sound transmission loss, J. Appl. Phys. 123 (2018). https://doi.org/10.1063/1.5025570.

[10] J.W. Jung, J.E. Kim, J.W. Lee, Acoustic metamaterial panel for both fluid

passage and broadband soundproofing in the audible frequency range, Appl. Phys. Lett. 112 (2018). https://doi.org/10.1063/1.5004605.

[11] P. Wu, Q. Mu, X. Wu, L. Wang, X. Li, Y. Zhou, S. Wang, Y. Huang, W. Wen, Acoustic absorbers at low frequency based on split-tube metamaterials, Phys. Lett. A 383 (2019) 2361–2366. https://doi.org/10.1016/j.physleta.2019.04.056.

[12] D. Qian, Z. Shi, Bandgap properties in locally resonant phononic crystal double panel structures with periodically attached spring–mass resonators, Phys. Lett. A 380 (2016) 3319–3325. https://doi.org/10.1016/j.physleta.2016.07.068.

[13] S. Wang, X. Zhang, F. Li, S.M. Hosseini, Sound transmission loss of a novel acoustic metamaterial sandwich panel: Theory and experiment, Appl. Acoust. 199 (2022) 109035. https://doi.org/10.1016/j.apacoust.2022.109035.

[14] J. Guo, Y. Xiao, H. Ren, H. Chen, D. Yu, J. Wen, Broadband low-frequency sound insulation of double-panel metastructures with a perforated lattice truss-core sandwich plate, Mech. Syst. Signal Process. 200 (2023) 110634. https://doi.org/10.1016/j.ymssp.2023.110634.

[15] V. Cool, O. Sigmund, N. Aage, F. Naets, E. Deckers, Vibroacoustic topology optimization for sound transmission minimization through sandwich structures, J. Sound Vib. 568 (2024) 117959. https://doi.org/10.1016/j.jsv.2023.117959.

[16] T.-T. Wu, Z.-G. Huang, T.-C. Tsai, T.-C. Wu, Evidence of complete band gap and resonances in a plate with periodic stubbed surface, Appl Phys Lett 93 (2008). https://doi.org/10.1063/1.2970992.

[17] Y. Pennec, B. Djafari-Rouhani, H. Larabi, J.O. Vasseur, A.C. Hladky-Hennion, Low-frequency gaps in a phononic crystal constituted of cylindrical dots deposited on a thin homogeneous plate, Phys Rev B 78 (2008) 104105. https://doi.org/10.1103/PhysRevB.78.104105.

[18] M. Oudich, Y. Li, B.M. Assouar, Z. Hou, A sonic band gap based on the locally resonant phononic plates with stubs, New J Phys 12 (2010) 083049. https://doi.org/10.1088/1367-2630/12/8/083049.

[19] Y. Li, T. Chen, X. Wang, Y. Xi, Q. Liang, Enlargement of locally resonant sonic band gap by using composite plate-type acoustic metamaterial, Phys. Lett. A 379

(2015) 412–416. https://doi.org/10.1016/j.physleta.2014.11.028.

[20] F. Langfeldt, W. Gleine, Optimizing the bandwidth of plate-type acoustic metamaterials, J. Acoust. Soc. Am. 148 (2020) 1304–1314. https://doi.org/10.1121/10.0001925.

[21] F. Langfeldt, W. Gleine, Plate-type acoustic metamaterials with strip masses, J. Acoust. Soc. Am. 149 (2021) 3727–3738. https://doi.org/10.1121/10.0005112.

[22] F. Langfeldt, A.J. Khatokar, W. Gleine, Plate-type acoustic metamaterials with integrated Helmholtz resonators, Appl. Acoust. 199 (2022) 109019. https://doi.org/10.1016/j.apacoust.2022.109019.

[23] J. Gu, Y. Tang, X. Wang, Z. Huang, Laminated plate-type acoustic metamaterials with Willis coupling effects for broadband low-frequency sound insulation, Compos. Struct. 292 (2022) 115689. https://doi.org/10.1016/j.compstruct.2022.115689.

[24] R.-S. Li, X.-W. Sun, X.-L. Gao, G.-G. Xu, T. Song, J.-H. Tian, Sound transmission loss overlay mechanism of plate-type acoustic metamaterials with Helmholtz resonators, Phys. Lett. A 538 (2025) 130358. https://doi.org/10.1016/j.physleta.2025.130358.

[25] S.J. Kline, Similitude and approximation theory, Springer Science & Business Media, 2012.

[26] M. Weisberg, Simulation and similarity: Using models to understand the world, Oxford University Press, 2012.

[27] W. Soedel, Similitude Approximations for Vibrating Thin Shells, J. Acoust. Soc. Am. 49 (1971) 1535–1541. https://doi.org/10.1121/1.1912530

[28] U.R. Kristiansen, W. Soedel, J.F. Hamilton, An investigation of scaling laws for vibrating beams and plates with special attention to the effects of shear and rotatory inertia, J. Sound Vib. 20 (1972) 113–122. https://doi.org/10.1016/0022-460X(72)90766-3.

[29] Y. Zhu, Y. Wang, Z. Luo, Q. Han, D. Wang, Similitude design for the vibration problems of plates and shells: A review, Front. Mech. Eng. 12 (2017) 253–264.

https://doi.org/10.1007/s11465-017-0418-1.

[30] G. Petrone, M. Manfredonia, S. De Rosa, F. Franco, Structural similitudes of stiffened cylinders, Math. Mech. Solids 24 (2019) 527–541. https://doi.org/10.1177/1081286517745722.

[31] A. Casaburo, G. Petrone, F. Franco, S. De Rosa, A Review of Similitude Methods for Structural Engineering, Appl. Mech. Rev. 71 (2019). https://doi.org/10.1115/1.4043787.

[32] Z. Yang, J. Mei, M. Yang, N.H. Chan, P. Sheng, Membrane-Type Acoustic Metamaterial with Negative Dynamic Mass, Phys. Rev. Lett. 101 (2008) 204301. https://doi.org/10.1103/PhysRevLett.101.204301.

[33] E. Ventsel, T. Krauthammer, E. Carrera, Thin Plates and Shells: Theory, Analysis, and Applications, Appl. Mech. Rev. 55 (2002) B72–B73. https://doi.org/10.1115/1.1483356.

[34] F. Langfeldt, J. Riecken, W. Gleine, O. von Estorff, A membrane-type acoustic metamaterial with adjustable acoustic properties, J. Sound Vib. 373 (2016) 1–18. https://doi.org/10.1016/j.jsv.2016.03.025.

[35] F. Langfeldt, On the validity of periodic boundary conditions for modelling finite plate-type acoustic metamaterials, J. Acoust. Soc. Am. 155 (2024) 837–845. https://doi.org/10.1121/10.0024619.

[36] Y. Xiao, J. Cao, S. Wang, J. Guo, J. Wen, H. Zhang, Sound transmission loss of plate-type metastructures: Semi-analytical modeling, elaborate analysis, and experimental validation, Mech. Syst. Signal Process. 153 (2021) 107487. https://doi.org/10.1016/j.ymssp.2020.107487.